



Cite this: *Chem. Commun.*, 2015, 51, 8421

Received 6th January 2015,
Accepted 19th February 2015

DOI: 10.1039/c5cc00113g

www.rsc.org/chemcomm

Separation of polar compounds using a flexible metal–organic framework†

Radha Kishan Motkuri,^{*a} Praveen K. Thallapally,^{*b} Harsha V. R. Annapureddy,^b Liem X. Dang,^b Rajamani Krishna,^{*c} Satish K. Nune,^a Carlos A. Fernandez,^a Jian Liu^a and B. Peter McGrail^a

A flexible metal–organic framework constructed from a flexible linker is shown to possess the capability of separating mixtures of polar compounds (propanol isomers) by exploiting the differences in the saturation capacities of the constituents. Transient breakthrough simulations show that these sorption-based separations are in favor of the component with higher saturation capacity.

Separation and purification of organic liquid isomers are scientifically important industrial technologies and have received considerable attention worldwide.¹ Distillation is clearly the dominating separation process, accounting for more applications than all the other chemical-separation processes combined. In fact, distillation columns consume more than 50% of the total energy used in the chemical industry worldwide. Even more challenging is separation of an azeotrope mixture that forms when certain compositions of liquid isomers are present by weight. Specifically, the separation of water, alcohols, and ketones is often made difficult because of azeotrope formation. Separating these mixtures using fractional distillation or using polymeric membranes is energy-intensive and is highly complex.² Alternatively, these processes sometimes require the addition of separating agents, called entrainers, that alter the vapor/liquid equilibrium in a favorable manner to achieve the desired separation, but the recovery of such entrainers later in the process not only requires an additional distillation step but also incurs an increased overall energy penalty. The largest opportunities for energy reduction in this area are offered by replacing distillation

or membrane-based separations by low-cost adsorption-based systems. The success of such replacement strategies is crucially dependent on the development of suitable adsorbents, but there is very limited information available on adsorption-based separation of azeotropes using porous media.

Recent developments in porous metal–organic frameworks (MOFs) have gained much attention because of the outstanding properties and ability to fine tune the pore apertures and high stability towards the desired application.^{3,4} Such remarkable properties of MOFs make them an interesting class of materials for adsorption,⁵ and separation applications.⁶ Specifically, studies of the gas separation are extensively reported in the literature; however, very limited information is available on the separation of polar molecules, including azeotropic mixtures. For example, Denayer *et al.* used highly stable zeolitic imidazole frameworks (ZIF-8, ZIF-68) to separate butanol from aqueous mixtures in the presence of organic contaminants like ethanol.⁷ Jie Zhang *et al.* reported the separation of alcohol and water mixtures using a charge-polarized MOF that shows selectivity towards polar molecules under an electric field gradient.⁸ Similarly, Kitagawa *et al.* synthesized a copper-based coordination polymer that selectively adsorbs methanol and water from bioethanol.⁹ Most of these studies focused on purifying bioethanol, but there are few reports that focus on the separation of mixtures of alcohols and other polar molecules such as chloroform and acetone.^{6g,10} Our experimental adsorption studies coupled with transient breakthrough simulations confirm the separation of propanol isomers and various azeotropes. To our knowledge, this is the first report on the separation of mixtures of propanol isomers and other binary mixtures containing alcohols, chloroform, and acetone using flexible MOFs.

TetZB, the flexible porous framework used in this communication, was synthesized using a flexible tetrahedral organic linker, tetrakis[4-(carboxyphenyl)-oxamethyl]methane **1** (Scheme S1, ESI†), and then was used effectively for the sorption and separation of polar solvents. The synthesis method and associated sorption properties of TetZB were reported by us previously.¹¹ For this study, we chose adsorption experiments of polar solvents such as C1–C3 alcohols, water, acetone, chloroform, and benzene, respectively.

^a Energy and Environment Directorate, Pacific Northwest National Laboratory (PNNL), Richland, WA 99352, USA. E-mail: radhakishan.motkuri@pnnl.gov

^b Fundamental and Computational Sciences Directorate, PNNL, Richland, WA 99352, USA. E-mail: praveen.thallapally@pnnl.gov

^c Van 't Hoff Institute for Molecular Sciences, University of Amsterdam, The Netherlands. E-mail: r.krishna@contact.uva.nl

† Electronic supplementary information (ESI) available: (a) Material synthesis, characterization; (b) pure component isotherms and dual-Langmuir–Freundlich models; (c) adsorption energy calculations; (d) GCMC simulation studies; (e) IAST calculations; (f) transient breakthrough simulation methodology; and (g) video animations for transient breakthroughs of several binary mixture separations. See DOI: 10.1039/c5cc00113g

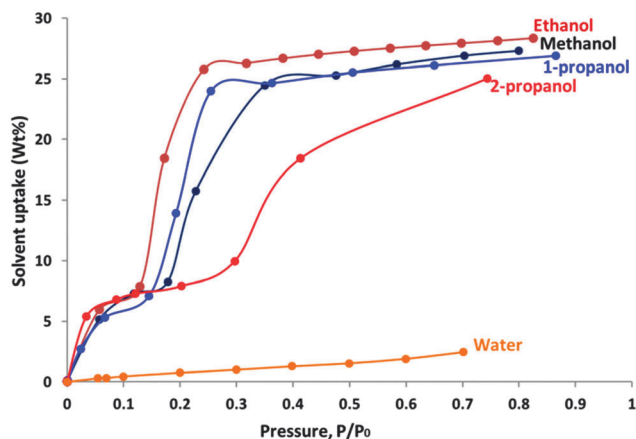


Fig. 1 Adsorption isotherms of alcohol adsorbents and water in TetZB at 298 K.

Experimentally measured vapor sorption capacities were obtained using an Intelligent Gravimetric Analyzer (IGA) from Hiden Instruments. The TetZB sample was activated at 473 K under dynamic vacuum before sorption studies. To evaluate the separation efficiency of TetZB, we initially considered 1-propanol/2-propanol isomers for the sorption studies. After sample activation, the MOF sample was exposed to 1-propanol vapors and the sorption behavior was plotted against pressure. The adsorption curve shows a sudden increase in uptake at a relative pressure (P/P_0) of 0.15 reaching the first saturation capacity of 7.8 wt%. At a relative pressure (P/P_0) of 0.27, TetZB shows another step adsorption reaching the second saturation capacity of 26 wt% or 4.55 mmol g^{-1} (Fig. 1). Such two-step adsorption was observed in TetZB with other gases/vapors and was shown to expand and contract the framework upon guest removal and re-adsorption of the same or different guest molecule. The flexibility arises from the twisting of benzoate moieties around the central quaternary carbon atom through ethereal links of the tetrahedral building block, which result from diverse ligand geometries such as tetrahedral, irregular, or near-flattened. Such building block flexibility has been observed both by us and other researchers. The desorption curve does not follow the adsorption, rather, it shows a sudden decrease in the sorption capacity at a P/P_0 ratio of 0.03 (Fig. S1, ESI†). Similarly, when a freshly activated MOF sample was exposed to 2-propanol vapors, the first uptake isotherm reached its first plateau at $P/P_0 = 0.3$; which was followed by a step adsorption with approximately 2.5 times higher capacity (25 wt%, 4.1 mmol g^{-1} at $P/P_0 = 0.8$), and then the saturation point was reached. Another significant difference between these two sorption isotherms is the rates at which they sorb onto the TetZB framework. Sorption profiles indicate that both propanol isomers can enter the pores of TetZB, but 1-propanol with its kinetic diameter of 4.7 Å has slightly higher uptake when compared to 2-propanol with the same kinetic diameter. This may be attributed to the flexibility of 1-propanol, which is a linear chain that can enter the pore more easily than a branched isomer. The density functional theory (DFT) estimated dipole moment value of 2-propanol is slightly higher (1.56D) than that of 1-propanol (1.49D), which shows that the 2-propanol molecule is more likely to be polarized by the TetZB pore structure, thus having a sharper uptake at relatively low pressure compared to 1-propanol.¹²

To gain further insights into sorption behavior, we performed grand canonical Monte Carlo (GCMC) simulations using the MuSic program where the simulation box consisted of one unit cell of MOF and the periodic boundary conditions were used in all three dimensions.¹³ Because the host framework considered has a rigid structure, the breathing phenomenon was not observed, but the overall solvent uptake matched the experimental results at 25 °C (Fig. S6, ESI†). In agreement with experimental results, the simulations of the 2-propanol sorption curve appear to be steeper at lower loadings when compared to 1-propanol. To understand this behavior, we computed the interaction energies between the TetZB framework and propanol isomers as a function of loading. The simulated results clearly showed more negative interaction energies for 2-propanol when compared to 1-propanol at lower loadings (Fig. S6, ESI†), but the overall uptake is slightly higher for 1-propanol. These intriguing experimental and simulation results suggest that vapor sorption experiments of 1-propanol and 2-propanol using the flexible TetZB have potential for separating propanol isomers, which motivated us to undertake further IAST breakthrough simulations (Fig. 2).

We then focused our attention on lower chain alcohols such as methanol and ethanol. The sorption isotherm of methanol shows a sudden increase at a P/P_0 ratio of 0.18 and then reaches

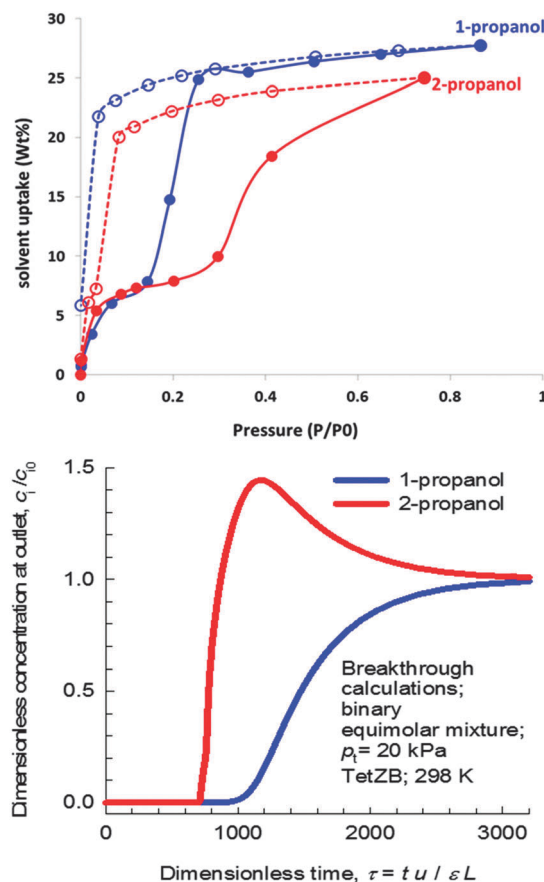


Fig. 2 Adsorption and desorption isotherms of 1-/2-propanol in TetZB (top) and the corresponding transient breakthrough simulation characteristics of an adsorber packed with TetZB for separation of 50/50 mixtures of 1-propanol from 2-propanol (bottom).

27 wt% at a P/P_0 ratio of 0.8. For ethanol after the first uptake at low relative pressure, the isotherm reaches its first plateau (7.8 wt% at a P/P_0 ratio of 0.12) followed by a step adsorption with approximately four times higher capacity of ethanol (25.7 wt%, 6 mmol g^{-1} at $P/P_0 = 0.25$). Because of the hydrophobic nature of the TetZB framework, water sorption studies show a low uptake until the P/P_0 ratio reaches 0.7, and the isotherm does not reach saturation even at a P/P_0 ratio of 0.95. The saturated loadings of alcohols decrease as the size increases from methanol to propanol because adsorption near saturation is mainly directed by the entropic (size) effect as fewer propanol molecules can be adsorbed compared to methanol (Fig. S2, ESI†). Furthermore, interestingly when TetZB is exposed to acetone vapors, the first plateau is reached at a very low relative pressure ($P/P_0 = 0.05$). Chloroform and benzene show a type-I isotherm that exhibits significant uptakes at low vapor pressures. The distinct behaviors of the solvent molecules with the host framework definitely reveal potential for application in separation technologies that should be studied.

To investigate the separation potential of TetZB, the experimentally measured loadings of 1- and 2-propanols, methanol, ethanol, acetone, benzene, chloroform, and water were fitted with the dual-site Langmuir–Freundlich model, and the fits are excellent over the entire range of pressures. The details of simulation methodology and the breakthrough simulations using IAST calculations are outlined in the ESI.† The transient breakthrough simulations suggest that TetZB has the potential to separate mixtures of alcohols by differentiating on the basis of chain length and conformation as can be observed for 1-propanol/2-propanol mixtures (Fig. S7–S9, ESI†). The separation of 1-propanol from 2-propanol is governed by molecular packing effects that favor the adsorption of the linear alcohol when operating under conditions corresponding to pore saturation. The better packing efficiency of 1-propanol is reflected in its higher saturation capacity compared to 2-propanol. It is important to note that this separation is not dictated by differences in binding energies that are higher for 2-propanol (Fig. S6b, ESI†). For other mixtures of 1-alcohols, in the Henry regime, at pressures below 1 kPa, selectivity favors alcohols with longer chain lengths; however, at pressures above 10 kPa, selectivity favors alcohols with shorter chain lengths. This is because of the higher saturation capacity of the shorter chain alcohols. The IAST calculations also imply that sharp separations of alcohol mixtures are possible using TetZB provided the operating pressures are greater than 10 kPa. This is confirmed in the transient breakthrough simulations presented for 50/50 mixtures of methanol/ethanol, ethanol/1-propanol, and ethanol/2-propanol at a total pressure of 100 kPa (Fig. 3, Fig. S9–S12, ESI†). It is interesting to compare the separations of TetZB with those obtained with ZIF-8 and CHA zeolites. The shorter chain alcohol is eluted later than the longer chain alcohol, which is in agreement with the corresponding results for other microporous materials such as SAPO-34, and ZIF-8 reported previously.^{7b,14} Comparisons of ethanol/1-propanol adsorption selectivity, and uptake capacity of ethanol for equimolar ethanol/1-propanol mixtures in TetZB, ZIF-8, and CHA zeolites are shown in Fig. S10 (ESI†). We note that TetZB

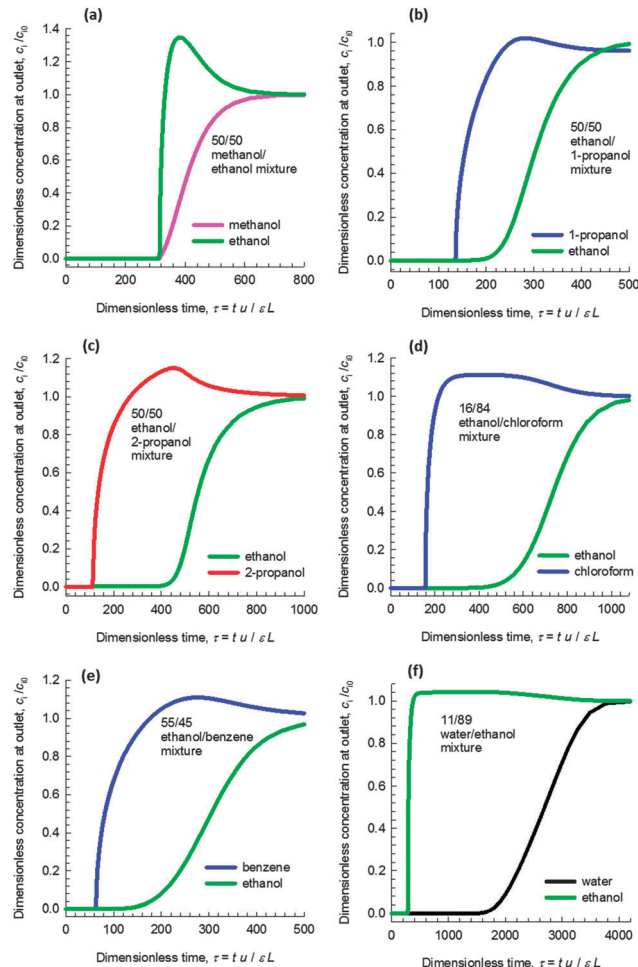


Fig. 3 Transient breakthrough simulation characteristics of an adsorber packed with TetZB for separation of ethanol from various solvent mixtures of (a) methanol, (b) 1-propanol, (c) 2-propanol, (d) chloroform, (e) benzene, (f) water at 298 K. The total pressure is 100 kPa.

has both higher selectivity and higher uptake capacity, making it more suitable for separation of mixtures of 1-alcohols (Fig. S11–S16, ESI†). Fig. 3f shows the separations of water–ethanol mixtures of azeotropic composition using TetZB. The separation is selective to water that has the higher saturation capacity; similar water-selective separations, achieved as a result of molecular packing effects, have been reported for CuBTC.¹⁵ The methodology adopted for the breakthrough simulations is provided in the ESI.† Also available in ESI† are seven video animations of the breakthroughs.

The experimental and modeling sorption analysis shows that the hydrophobic $-\text{CH}_2$ and aryl groups of tectonic acid and phenyl groups of the 4,4'-bipyridine molecules are exposed inside the pore, thereby creating a hydrophobic environment.¹¹ To illustrate such an environment, we painted all the hydrophobic groups in green and the hydrophilic groups in red where it is clearly evident that hydrophobic groups dominate the surface of the pore (Scheme S1, Fig. S6, ESI†). The metal atoms and the carboxylate groups that are more hydrophilic are buried deep inside and are not easily accessible to the guest molecules. Polar alcohol, such as methanol and ethanol, molecules consisting of hydrophobic and

hydrophilic groups interact favorably with pore components, leading to higher uptake rates with high adsorption energies. To our knowledge, this is the first report of the separation of propanol isomers, mixtures of 1-alcohols with acetone, and chloroform ketones using MOFs.

In conclusion, we reported that hydrophobic TetZB, a flexible metal organic framework generated from a flexible tetrahedral building block, shows remarkable affinity and separation capability of alcohols and ketones, specifically separation of propanol isomers. If the operating conditions are chosen such that pore saturation is achieved, separation using TetZB strongly favors the component with the higher saturation capacity. For mixtures of alcohols, the separation is selective for the alcohols with the shorter chain length. For separation of water–alcohol mixtures, the separation favors water. Of particular interest is the separation of azeotropic water–ethanol mixtures; see Fig. 3(f).

This work was performed at the Pacific Northwest National Laboratory (PNNL) and was supported by the U.S. Department of Energy (DOE). L.X.D. acknowledges funding from the U.S. Department of Energy, Office of Science, Office of Basic Energy Sciences, Division of Chemical Sciences, Geosciences, and Biosciences. PNNL is operated by Battelle for the U.S. Department of Energy under Contract DE-AC05-76RL01830.

Notes and references

- 1 Industrial Technologies Program; US-DOE EERE, 2005, 14.
- 2 F. P. Mccandless and W. B. Downs, *J. Membr. Sci.*, 1987, **30**, 111–116.
- 3 (a) O. K. Farha, C. E. Wilmer, I. Eryazici, B. G. Hauser, P. A. Parilla, K. O'Neill, A. A. Sarjeant, S. T. Nguyen, R. Q. Snurr and J. T. Hupp, *J. Am. Chem. Soc.*, 2012, **134**, 9860–9863; (b) M. Eddaoudi, J. Kim, N. Rosi, D. Vodak, J. Wachter, M. O'Keeffe and O. M. Yaghi, *Science*, 2002, **295**, 469–472; (c) H. X. Deng, S. Grunder, K. E. Cordova, C. Valente, H. Furukawa, M. Hmadeh, F. Gandara, A. C. Whalley, Z. Liu, S. Asahina, H. Kazumori, M. O'Keeffe, O. Terasaki, J. F. Stoddart and O. M. Yaghi, *Science*, 2012, **336**, 1018–1023; (d) G. Ferey, *Chem. Soc. Rev.*, 2008, **37**, 191–214; (e) N. Stock and S. Biswas, *Chem. Rev.*, 2012, **112**, 933–969; (f) D. Banerjee, A. J. Cains, J. Liu, R. K. Motkuri, S. K. Nune, C. A. Fernandez, R. Krishna, D. M. Strachan and P. K. Thallapally, *Acc. Chem. Res.*, 2015, **48**, 211–219.
- 4 (a) J. R. Li, J. Sculley and H. C. Zhou, *Chem. Rev.*, 2012, **112**, 869–932; (b) H. Furukawa, K. E. Cordova, M. O'Keeffe and O. M. Yaghi, *Science*, 2013, **341**, 1230444; (c) T. Li, M. T. Kozlowski, E. A. Doud, M. N. Blakely and N. L. Rosi, *J. Am. Chem. Soc.*, 2013, **135**, 11688–11691; (d) R. Haldar, S. K. Reddy, V. M. Suresh, S. Mohapatra, S. Balasubramanian and T. K. Maji, *Chem. – Eur. J.*, 2014, **20**, 4347–4356; (e) R. K. Motkuri, J. Liu, C. A. Fernandez, S. K. Nune, P. Thallapally and B. P. McGrail, *Industrial Catalysis and Separations*, Apple Academic Press, 2014, pp. 61–103.
- 5 H. T. Kwon and H. K. Jeong, *J. Am. Chem. Soc.*, 2013, **135**, 10763–10768.
- 6 (a) R. K. Motkuri, H. V. R. Annapureddy, M. Vijaykumar, H. T. Schaef, P. F. Martin, B. P. McGrail, L. X. Dang, R. Krishna and P. K. Thallapally, *Nat. Commun.*, 2014, **5**, 4368; (b) Z. Y. Gu and X. P. Yan, *Angew. Chem., Int. Ed.*, 2010, **49**, 1477–1480; (c) Z. R. Herm, B. M. Wiers, J. A. Mason, J. M. van Baten, M. R. Hudson, P. Zajdel, C. M. Brown, N. Masciocchi, R. Krishna and J. R. Long, *Science*, 2013, **340**, 960–964; (d) M. Latroche, S. Surble, C. Serre, C. Mellot-Draznieks, P. L. Llewellyn, J. H. Lee, J. S. Chang, S. H. Chung and G. Ferey, *Angew. Chem., Int. Ed.*, 2006, **45**, 8227–8231; (e) Z. Y. Gu, C. X. Yang, N. Chang and X. P. Yan, *Acc. Chem. Res.*, 2012, **45**, 734–745; (f) L. C. Lin, J. Kim, X. Q. Kong, E. Scott, T. M. McDonald, J. R. Long, J. A. Reimer and B. Smit, *Angew. Chem., Int. Ed.*, 2013, **52**, 4410–4413; (g) Z. J. Lin, R. Q. Zou, J. Liang, W. Xia, D. G. Xia, Y. X. Wang, J. H. Lin, T. L. Hu, Q. Chen, X. D. Wang, Y. S. Zhao and A. K. Burrell, *J. Mater. Chem.*, 2012, **22**, 7813–7818; (h) P. Pachfule, Y. F. Chen, J. W. Jiang and R. Banerjee, *Chem. – Eur. J.*, 2012, **18**, 688–694; (i) N. Chang, Z. Y. Gu and X. P. Yan, *J. Am. Chem. Soc.*, 2010, **132**, 13645–13647; (j) R. Krishna, *Phys. Chem. Chem. Phys.*, 2015, **17**, 39–59.
- 7 (a) S. Van der Perre, T. Van Assche, B. Bozbiyik, J. Lannoeye, D. E. De Vos, G. V. Baron and J. F. M. Denayer, *Langmuir*, 2014, **30**, 8416–8424; (b) J. C. Saint Remi, T. Remy, V. Van Hunskerken, S. van de Perre, T. Duerinck, M. Maes, D. De Vos, E. Gobechiya, C. E. A. Kirschhock, G. V. Baron and J. F. M. Denayer, *ChemSusChem*, 2011, **4**, 1074–1077.
- 8 J. K. Sun, M. Ji, C. Chen, W. G. Wang, P. Wang, R. P. Chen and J. Zhang, *Chem. Commun.*, 2013, **49**, 1624–1626.
- 9 A. Shigematsu, T. Yamada and H. Kitagawa, *J. Am. Chem. Soc.*, 2012, **134**, 13145–13147.
- 10 (a) X. F. Zheng, L. Zhou, Y. M. Huang, C. G. Wang, J. G. Duan, L. L. Wen, Z. F. Tian and D. F. Li, *J. Mater. Chem. A*, 2014, **2**, 12413–12422; (b) K. Zhang, L. L. Zhang and J. W. Jiang, *J. Phys. Chem. C*, 2013, **117**, 25628–25635; (c) T. Borjigin, F. X. Sun, J. L. Zhang, K. Cai, H. Ren and G. S. Zhu, *Chem. Commun.*, 2012, **48**, 7613–7615.
- 11 (a) P. K. Thallapally, J. Tian, M. R. Kishan, C. A. Fernandez, S. J. Dalgarno, P. B. McGrail, J. E. Warren and J. L. Atwood, *J. Am. Chem. Soc.*, 2008, **130**, 16842–16843; (b) R. K. Motkuri, P. K. Thallapally, S. K. Nune, C. A. Fernandez, B. P. McGrail and J. L. Atwood, *Chem. Commun.*, 2011, **47**, 7077–7079.
- 12 M. Sadakiyo, T. Yamada and H. Kitagawa, *J. Am. Chem. Soc.*, 2011, **133**, 11050–11053.
- 13 A. Gupta, S. Chempath, M. J. Sanborn, L. A. Clark and R. Q. Snurr, *Mol. Simul.*, 2003, **29**, 29–46.
- 14 (a) R. Krishna and J. M. van Baten, *Sep. Purif. Technol.*, 2011, **76**, 325–330; (b) T. Remy, J. C. Saint Remi, R. Singh, P. A. Webley, G. V. Baron and J. F. M. Denayer, *J. Phys. Chem. C*, 2011, **115**, 8117–8125; (c) R. Krishna, *Microporous Mesoporous Mater.*, 2014, **185**, 30–50.
- 15 J. J. Gutierrez-Sevillano, S. Calero and R. Krishna, *J. Phys. Chem. C*, 2015, **119**, 3658–3666.

Electronic supplementary information (ESI) for

Separating mixtures of polar compounds using a flexible metal-organic framework

Radha Kishan Motkuri,^{*,†} *Praveen K. Thallapally*,^{*,‡} *Harsha. V. R. Annapureddy*,[‡] *Liem Dang*,[‡] *Rajamani Krishna*,^{*,II} *Satish K Nune*,[†] *Carlos. A. Fernandez*, *Jian Liu*,[†] *B. Peter McGrail*,[†]

[†] Energy and Environment Directorate, Pacific Northwest National Laboratory, Richland, WA 99352, USA.

[‡] Fundamental and Computational Sciences Directorate, Pacific Northwest National Laboratory, Richland, WA 99352, USA.

^{II} Van 't Hoff Institute for Molecular Sciences, University of Amsterdam, Science Park 904, 1098 XH Amsterdam, The Netherlands

*To whom correspondence: Radhakishan.Motkuri@pnnl.gov; praveen.thallapally@pnnl.gov; R.Krishna@contact.uva.nl

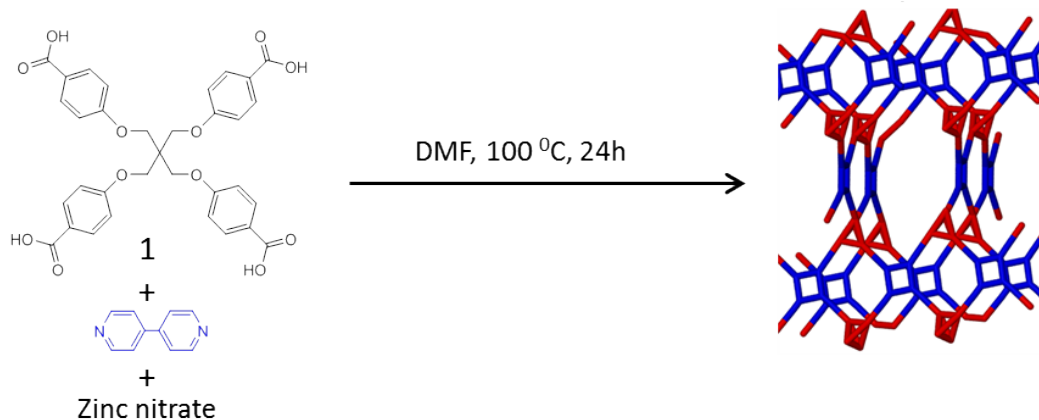
Table of Contents

Section S1.	Materials and Methods.....	2
Section S2.	Sorption isotherms of various polar solvents in TetZB.....	3
Section S3.	GCMC modeling studies.....	9
Section S4.	Fitting of pure component isothermes for TetZB.....	10
Section S5.	Simulation methodology for transient breakthrough in fixed bed adsorbers.....	11
Section S6.	Schematic of adsorber packed with TetZB for breakthrough simulations	21
Section S7.	Explanation on the Video animations.....	21
Section S8.	Notation.....	22
Section S9.	References.....	24

Section S1: Materials and Methods

Experimental Procedure:

TetZB (Scheme 1): The flexible tetrahedral organic linker **1** was successfully synthesized using a reported procedure, and further synthesis of TetZB MOF was reported by us previously.¹ Briefly, a solid mixture of flexible linker **1** (0.06 g, 0.1mmol, 1 equiv), bipyridine (0.015 g, 0.1mmol, 1 equiv, Aldrich), and $\text{Zn}(\text{NO}_3)_2 \cdot 6\text{H}_2\text{O}$ (0.03 g, 0.1 mmol, 1 equiv, Aldrich) was dissolved in 10 mL DMF in a 20 mL vial. The reaction mixture was mixed thoroughly and ultrasonicated until it became clear. The reaction vial was capped tightly and placed in an oven at 100 °C. After 24 hours, the sample was removed from the oven and allowed to cool to room temperature (RT). The mother liquor was decanted to obtain transparent crystals that then were washed with DMF (3 mL \times 3) and dried in air for 10 min.



Scheme S1

Section S2. Sorption isotherms of various polar solvents in TetZB:

Prior to measuring adsorption, the TetZB sample was placed in a container of the IGA chamber and the weight of the sample was recorded before activation. The temperature of the furnace was increased up to 250°C under vacuum at a rate of 5°C/min to remove the trapped solvent molecules. The sample was cooled to RT, its dry mass was set, and the experimental temperature 25°C was maintained by the IGA water bath. The static mode of the IGA was used to measure the sorption of polar solvents isotherms. The pressure points were set beforehand using the IGA software. The pressure was maintained at the set point by active computer control of the inlet/outlet valves throughout the duration of the experiment. Weight increases resulting from adsorption at each pressure step were plotted against the pressure.

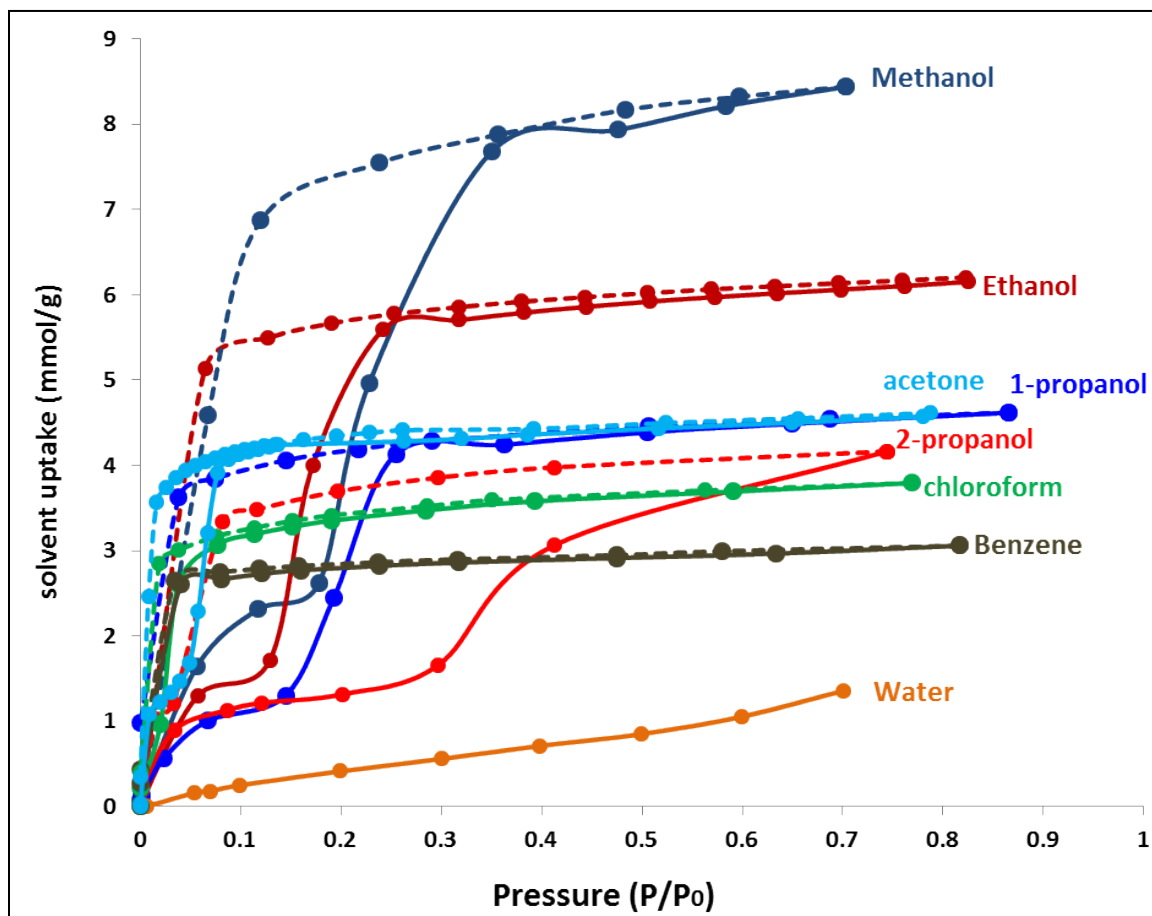


Figure S1: Reversible adsorption and desorption (mmol/g) isotherms of various polar solvents in TetZB at 25°C.

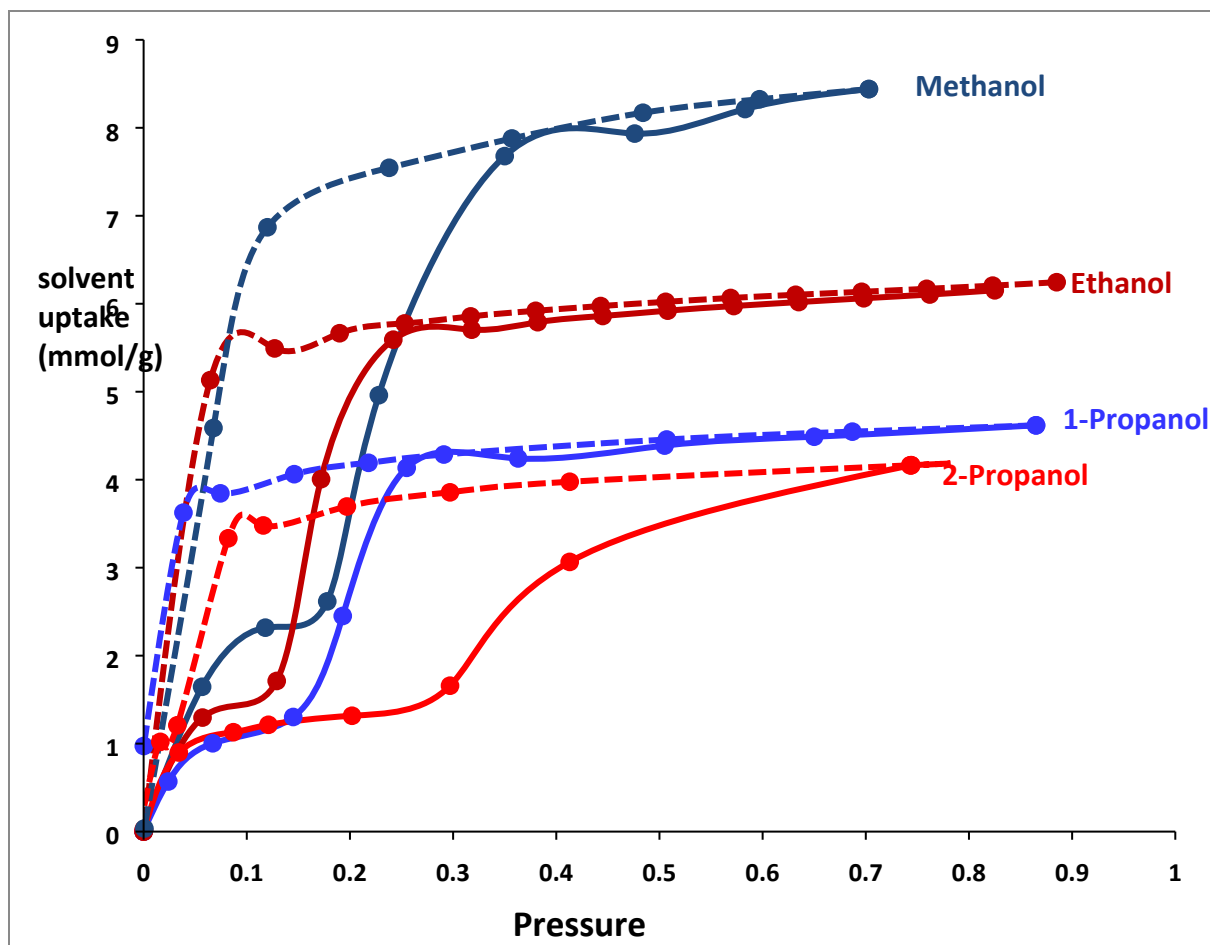


Figure S2: Reversible adsorption and desorption in mmol/g of C1–C3 alcohols at RT.

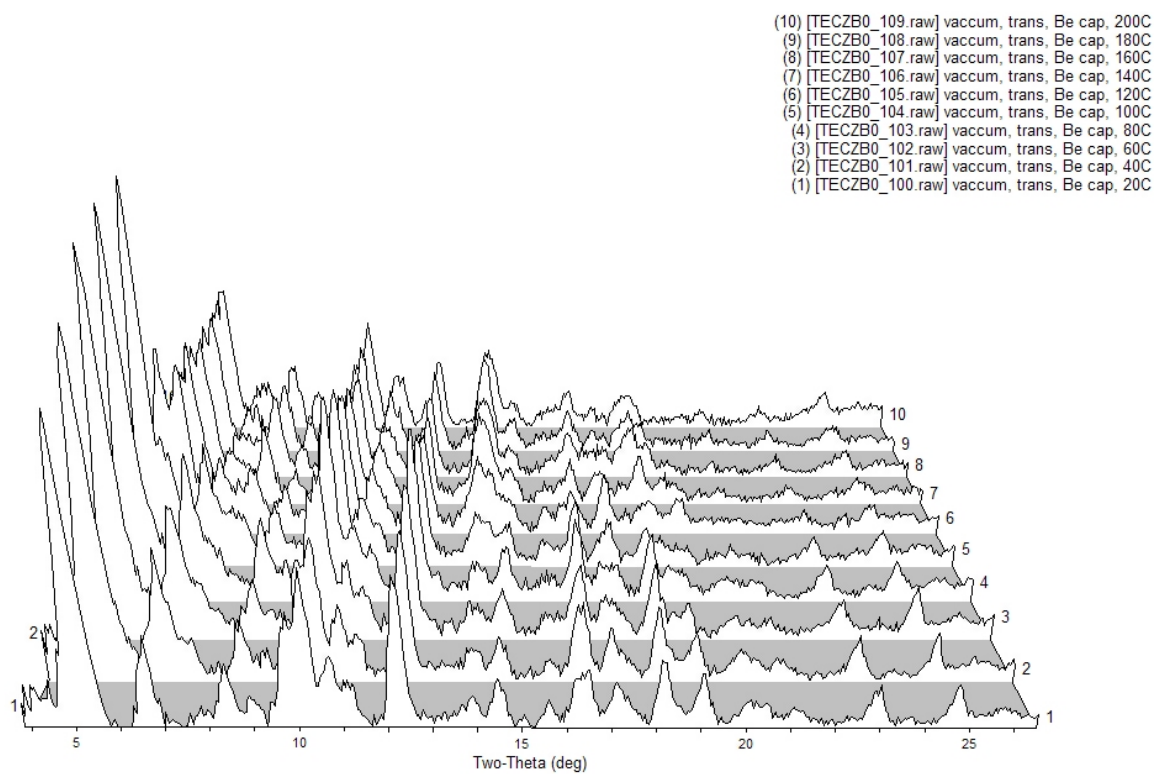


Figure S3: Powder XRD of the sample TetZB from 25°C to 200°C. Note the change in structure at 140°C.

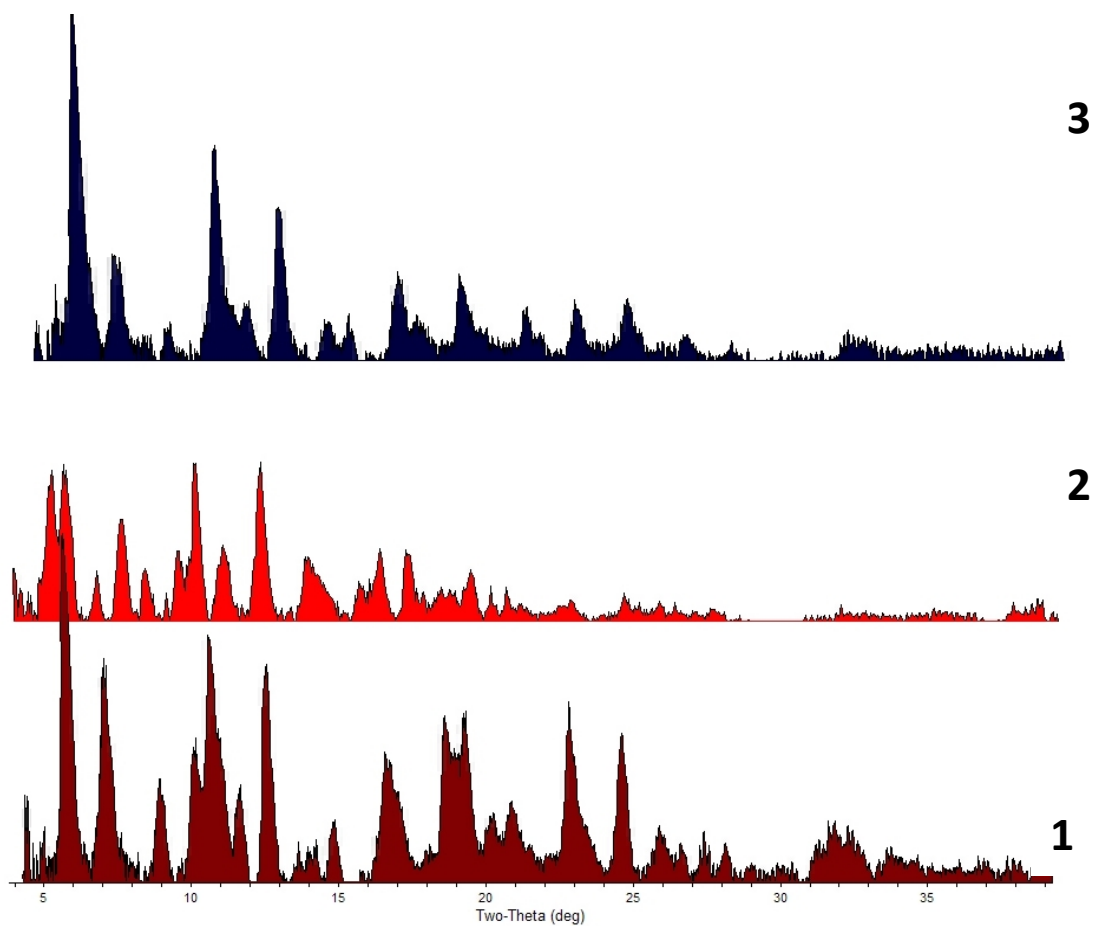


Figure S4. Powder XRD spectra of TetZB at (1) RT, (2) heated at 200°C under vacuum, and (3) exposed to methanol vapors for 24 hours.

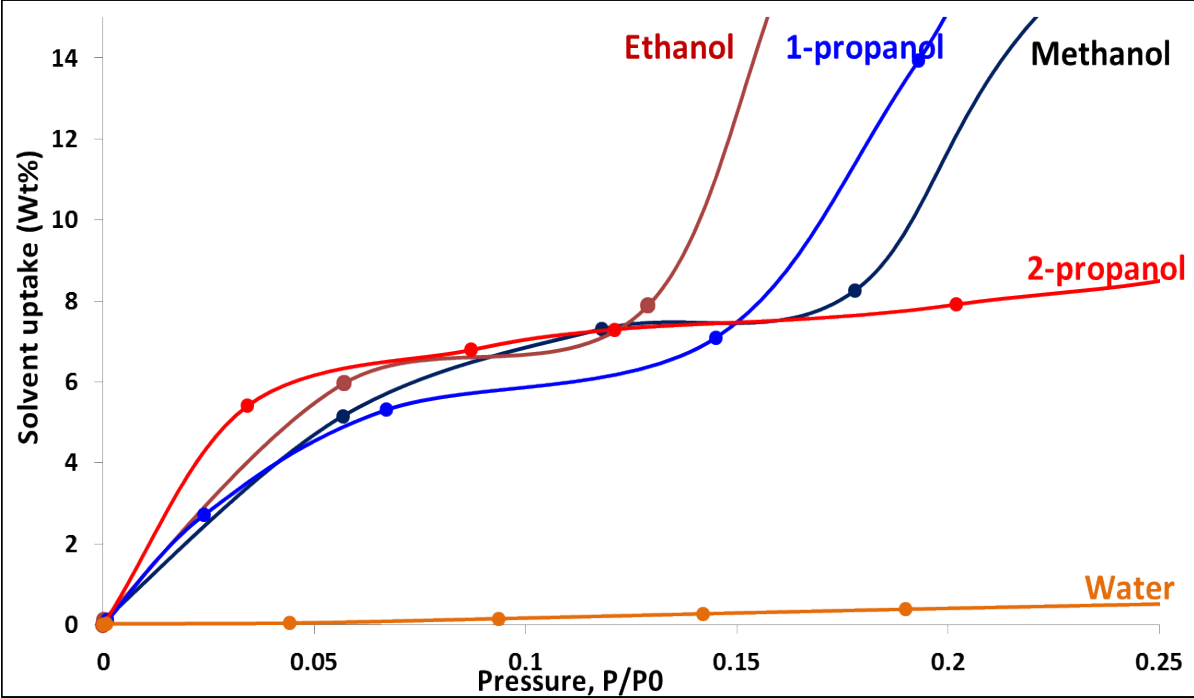
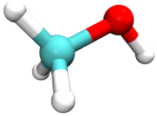
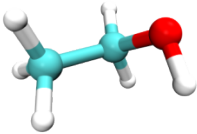
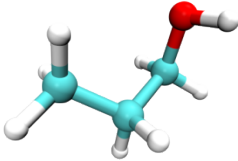
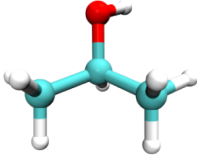



Figure S5: The expanded low partial pressure region of alcohols sorption isotherms in TetZB at 298K.

Table S1: Fundamental properties of adsorbents and their experimental sorption capacities in activated TetZB at 298K. Sorption capacities in wt% and corresponding values in mmol/g are provided for clarity. The dipole moments were taken from the reference Kitagawa et al 2011.²

Adsorbents	Structure	Kinetic diameter (Å)	Dipole moment (D)	Experimental Uptake wt% (mmol/g)
Methanol		3.6-4.0	1.69	27.0 (8.44)
Ethanol		4.3-4.5	1.71	28.3(6.15)
1-propanol		4.7	1.49	27.7 (4.6)
2-propanol		4.7	1.56	25.0 (4.16)
Water		2.6-2.9	1.86	2.44 (1.35)

Section S3: Grand Canonical Monte Carlo (GCMC) Modeling Studies:

To increase computational efficiency, the TetZB structure and the guest molecules are assumed to be rigid. Intermolecular interactions between the MOF framework and guest molecules were described by Lennard-Jones (LJ) and electrostatic interactions. GCMC simulations were performed with four types of moves: 1) molecular displacement, 2) molecular rotation, 3) insertion of a molecule with random orientation into a random position in the system, and 4) deletion of a randomly chosen molecule from the system. At each pressure point, we performed 2×10^7 trial moves for GCMC simulations. Because the host framework considered has a rigid structure, the breathing phenomenon was not observed; however, the overall uptake of the solvents matched the experimental results at 25°C. In the case of propanol isomers, both simulations and experiments show that the adsorption isotherm for 2-propanol was steeper at lower loadings compared to 1-propanol. To understand this behavior, we computed the interaction energies between MOF and propanol isomers as a function of loading. We obtained more negative interaction energies for 2-propanol compared to 1-propanol, which clearly indicates stronger a interaction between TetZB and 2-propanol at lower loadings, but overall, the observed loading for 1-propanol was slightly higher.

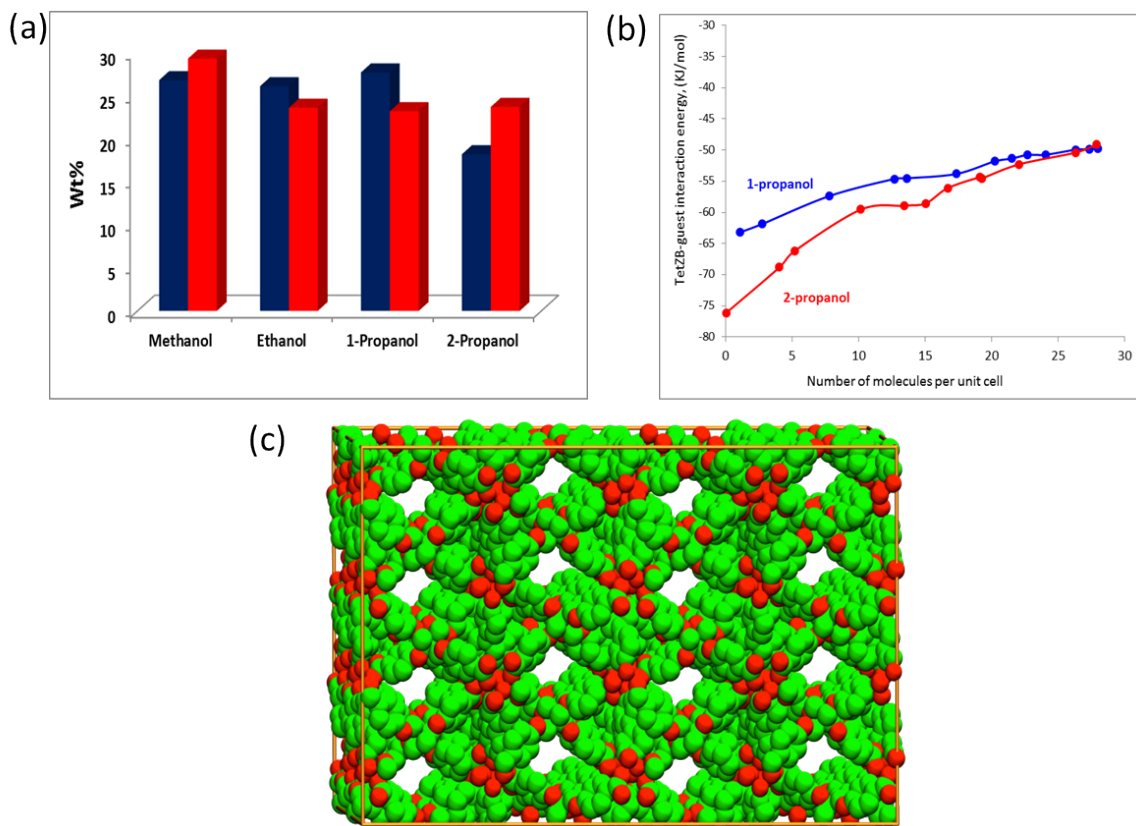


Figure S6: (a) Comparison of experimental (blue) vs. modeling (red) sorption studies of solvents in TetZB at $P/P_0=0.7$; (b) TetZB-guest 1-/2-propanol interaction energy calculations at lower loadings; (c) TetZB structure showing aromatic hydrophobic (green) and metallic (hydrophilic-red) in CPK model.

Section S4: Fitting of Isotherms:

The experimentally measured loadings of water, methanol, ethanol, 1-propanol, 2-propanol, acetone, benzene, and chloroform in TetZB obtained at RT (i.e., 298 K) were fitted with the dual-site Langmuir-Freundlich model.

$$q = q_{A,sat} \frac{b_A p^{V_A}}{1 + b_A p^{V_A}} + q_{B,sat} \frac{b_B p^{V_B}}{1 + b_B p^{V_B}} \quad (1)$$

The Langmuir-Freundlich parameters are provided in Table S2. Figure S4 provides a comparison of the pure component isotherm data with dual-site Langmuir-Freundlich fits. The

isotherms of all guest adsorbates water, methanol, ethanol, 1-propanol, 2-propanol, acetone, benzene and chloroform exhibit steep increases. Such steep increases are traceable to molecular clustering effects induced by hydrogen bonding; this has been established in the publications of Krishna and van Baten.³ To properly capture the steep isotherms, the Freundlich exponent needs to have large values in the range of 5 to 10.

The pure component isotherm data for water extends only to $p/p_0 = 0.95$ at which the saturation capacity is not reached. Consequently, the uncertainties for isotherm fits for water are significant. Nevertheless, the calculations presented below for adsorption equilibrium, and breakthroughs are expected to be of reasonable accuracy.

Section S5: Simulation Methodology for Transient Breakthrough in Fixed-Bed Adsorbers

Fixed bed adsorbers packed with crystals of microporous materials are commonly used for separation of mixtures; such adsorbers are commonly operated in a transient mode, and the compositions of the gas phase and the component loadings within the crystals vary with position and time. During the initial stages of the transience, the pores are loaded gradually, and only towards the end of the adsorption cycle are conditions corresponding to pore saturation achieved. In other words, separations in a fixed bed adsorber are influenced by both the Henry regime of adsorption as well as the conditions corresponding to pore saturation. Experimental data on the transient breakthrough of mixtures across fixed beds are commonly used to evaluate and compare the separation performance of zeolites and MOFs.⁴ For a given separation task, transient breakthroughs provide more a realistic evaluation of the efficacy of a material, as they reflect the combined influence of adsorption selectivity, adsorption capacity, and intra-crystalline diffusion limitations.^{4e, 5}

We describe below the simulation methodology used to perform transient breakthrough calculations that are presented in this work. This simulation methodology is the same as that used in our previously published work.^{4e}

Assuming plug flow of an n -component gas mixture through a fixed bed maintained under isothermal conditions, the partial pressures in the gas phase at any position and instant of time

are obtained by solving the following set of partial differential equations for each of the species i in the gas mixture.⁶

$$\frac{1}{RT} \frac{\partial p_i(t, z)}{\partial t} = -\frac{1}{RT} \frac{\partial (v(t, z) p_i(t, z))}{\partial z} - \frac{(1-\varepsilon)}{\varepsilon} \rho \frac{\partial \bar{q}_i(t, z)}{\partial t}; \quad i = 1, 2, \dots, n \quad (2)$$

In equation (2), t is the time, z is the distance along the adsorber, ρ is the framework density, ε is the bed void volume, v is the interstitial gas velocity, and $\bar{q}_i(t, z)$ is the *spatially averaged* molar loading within the crystallites of radius r_c , monitored at position z , and at time t .

At any time t , during the transient approach to thermodynamic equilibrium, the spatially averaged molar loading within the crystallite r_c is obtained by integration of the radial loading profile.

$$\bar{q}_i(t) = \frac{3}{r_c^3} \int_0^{r_c} q_i(r, t) r^2 dr \quad (3)$$

For transient unary uptake within a crystal at any position and time with the fixed bed, the radial distribution of molar loadings, q_i , within a spherical crystallite, of radius r_c , is obtained from a solution of a set of differential equations describing the uptake

$$\frac{\partial q_i(r, t)}{\partial t} = -\frac{1}{\rho} \frac{1}{r^2} \frac{\partial}{\partial r} (r^2 N_i) \quad (4)$$

The molar flux N_i of component i is described by the simplified version of the Maxwell-Stefan equations in which both correlation effects and thermodynamic coupling effects are considered to be of negligible importance.^{4e}

$$N_i = -\rho D_i \frac{\partial q_i}{\partial r} \quad (5)$$

Summing equation (3) over all n species in the mixture allows calculation of the *total average* molar loading of the mixture within the crystallite.

$$\bar{q}_t(t, z) = \sum_{i=1}^n \bar{q}_i(t, z) \quad (6)$$

The *interstitial* gas velocity is related to the *superficial* gas velocity by equation (7).

$$v = \frac{u}{\varepsilon} \quad (7)$$

In industrial practice, the most common operation is to use a step-wise input of mixtures to be separated into an adsorber bed that is initially free of adsorbates; that is, with the initial condition described by equation (8).

$$t = 0; \quad q_i(0, z) = 0 \quad (8)$$

At time, $t = 0$, the inlet to the adsorber, $z = 0$, is subjected to a step input of the n -component gas mixture, and this step input is maintained until the end of the adsorption cycle when steady-state conditions are reached.

$$t \geq 0; \quad p_i(0, t) = p_{i0}; \quad u(0, t) = u \quad (9)$$

where u is the superficial gas velocity at the inlet to the adsorber.

If the value of $\frac{D_i}{r_c^2}$ is large enough to ensure that intra-crystalline gradients are absent and the entire crystallite particle can be considered to be in thermodynamic equilibrium with the surrounding bulk gas phase at that time t , and position z of the adsorber

$$\bar{q}_i(t, z) = q_i(t, z) \quad (10)$$

The molar loadings at the *outer surface* of the crystallites (i.e., at $r = r_c$.) are calculated on the basis of adsorption equilibrium with the bulk gas phase partial pressures p_i at that position z and time t . The adsorption equilibrium can be calculated on the basis of the Ideal Adsorbed Solution Theory (IAST) of Myers and Prausnitz.⁷

For presenting the breakthrough simulation results, we use the dimensionless time, $\tau = \frac{tu}{L\varepsilon}$, obtained by dividing the actual time, t , by the characteristic time, $\frac{L\varepsilon}{u}$, where L is the length of

adsorber, u is the superficial fluid velocity, ε is the bed voidage.⁵ For all the simulations reported in this article, we choose $L = 0.3$ m; $u = 0.04$ m s⁻¹; $\varepsilon = 0.4$.

Table S2: Dual-site Langmuir-Freundlich parameters for adsorption of water, methanol, ethanol, 1-propanol, 2-propanol, chloroform, benzene, and acetone at 298 K in TetZB. These fits are for the “adsorption” branch of the isotherms.

Adsorbate	Site A			Site B		
	$q_{A,sat}$ mol kg ⁻¹	b_{A0} Pa ^{-ν_A}	\square_A dimensionless	$q_{B,sat}$ mol kg ⁻¹	b_{B0} Pa ^{-ν_B}	\square_B dimensionless
Water	3	4.01×10^{-5}	0.94	18	3.02×10^{-46}	13
Methanol	4.6	1.28×10^{-36}	10	6	5.08×10^{-3}	0.62
Ethanol	3.6	3.97×10^{-38}	12	3.2	8.4×10^{-3}	0.7
1-propanol	2.7	5.92×10^{-35}	12.5	2.5	2.79×10^{-2}	0.6
2-propanol	2.7	4.83×10^{-27}	7.8	1.7	4.43×10^{-2}	0.6
Chloroform	1.75	1.22×10^{-39}	13.2	2.7	4.76×10^{-2}	0.4
Benzene	1.6	1×10^{-36}	17.5	17	2.97×10^{-2}	0.12
Acetone	3	6.48×10^{-14}	4	2.6	2.49×10^{-1}	0.2

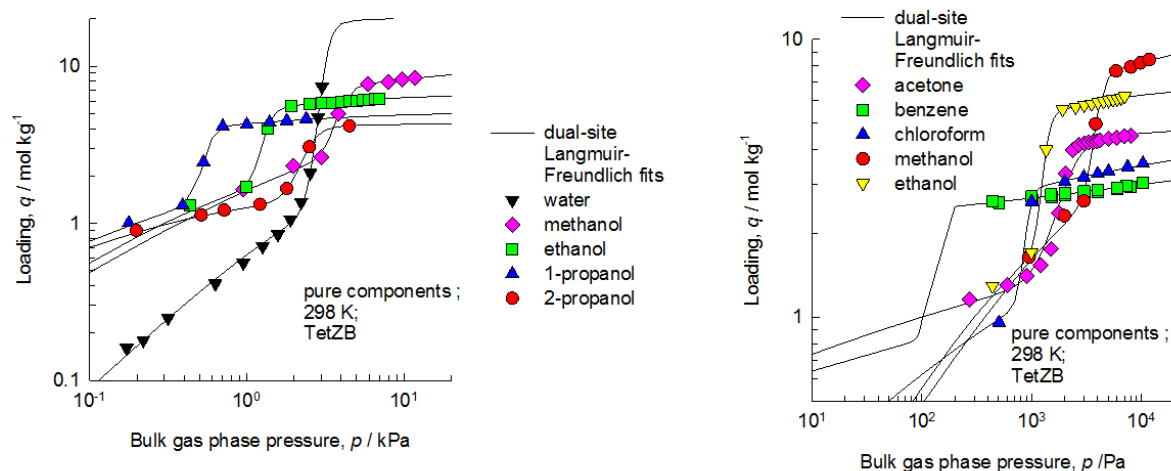


Figure S7. Comparison of the pure component isotherm data with dual-site Langmuir-Freundlich fits (parameters as provided in Table S2) or adsorption of water, methanol, ethanol, 1-propanol, 2-propanol, acetone, benzene, and chloroform in TetZB obtained at 298 K.

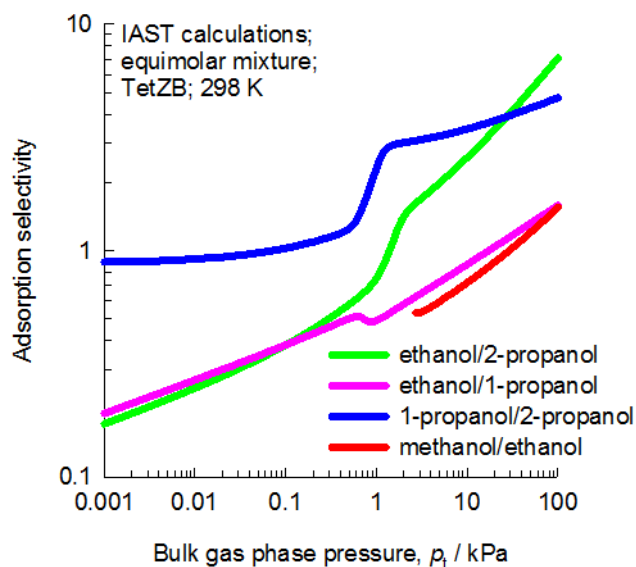


Figure S8. IAST calculations for binary adsorption equilibrium for equimolar methanol/ethanol, 1-propanol/2-propanol, ethanol/1-propanol, and ethanol/2-propanol in TetZB at 298 K.

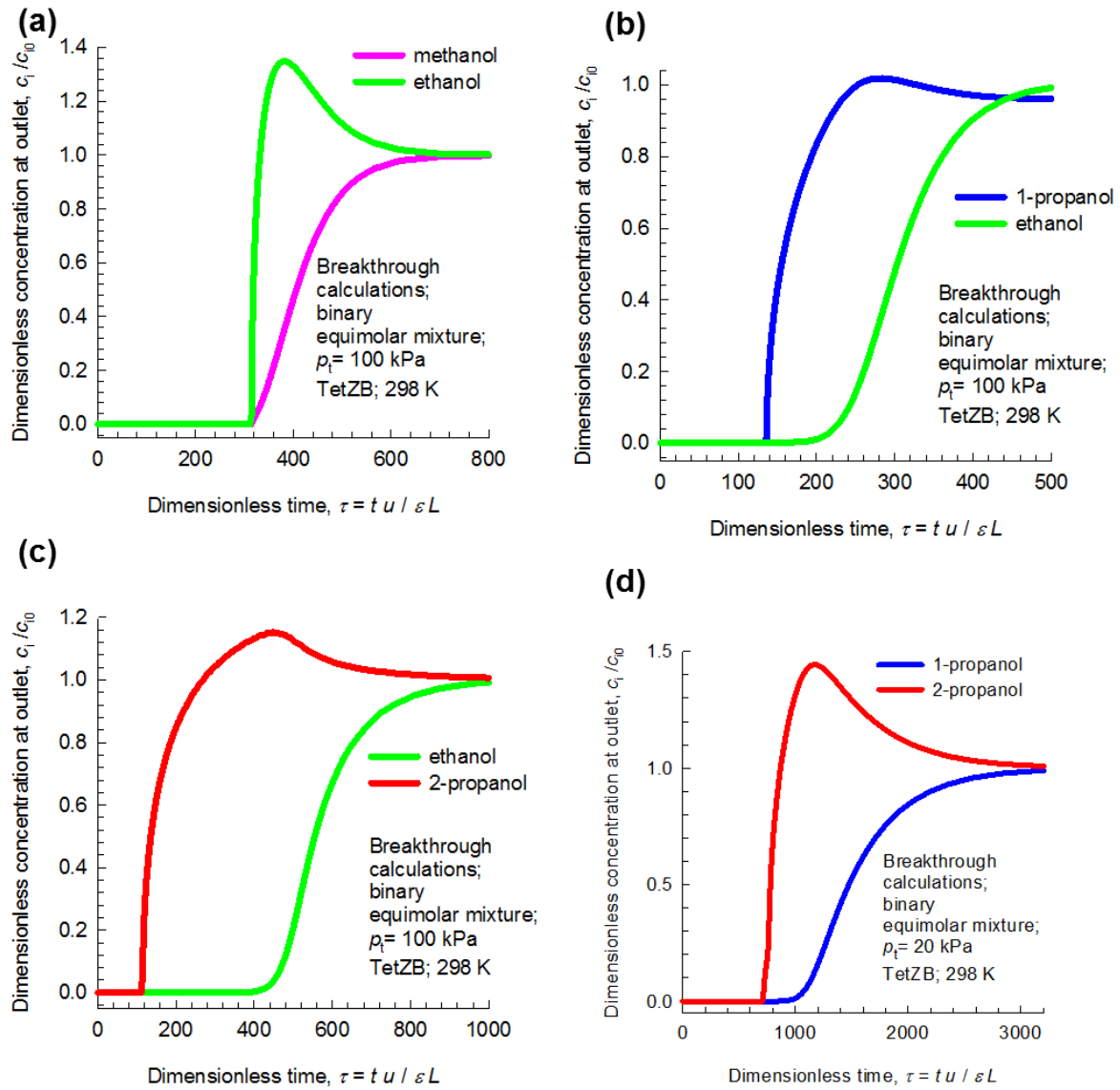


Figure S9. Transient breakthrough simulations for (a) 50/50 methanol/ethanol, (b) 50/50 ethanol/1-propanol, (c) 50/50 ethanol/2-propanol, and (d) 50/50 1-propanol/2-propanol mixture in a fixed-bed adsorber packed with TetZB at 298 K. In (a), (b), and (c), the total pressure is 100 kPa; in (d), the total pressure is 20 kPa. Intra-crystalline diffusion effects are accounted for by taking $D_{\text{methanol}}/r_c^2 = 2 \times 10^{-3} \text{ s}^{-1}$; $D_{\text{ethanol}}/r_c^2 = 1 \times 10^{-3} \text{ s}^{-1}$; $D_{\text{1-propanol}}/r_c^2 = D_{\text{2-propanol}}/r_c^2 = 1 \times 10^{-4} \text{ s}^{-1}$.

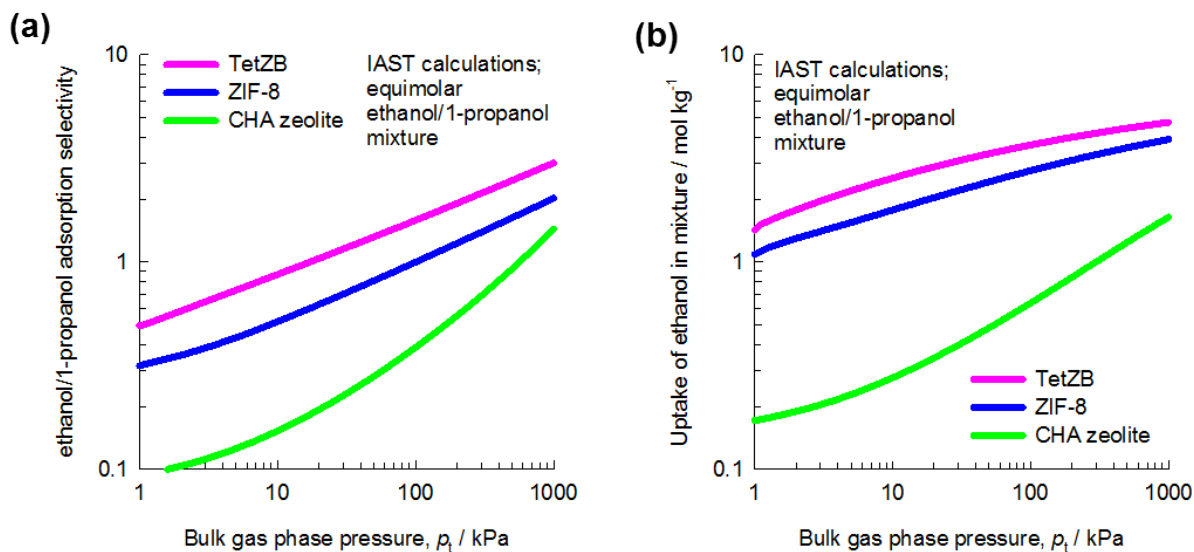


Figure S10. Comparison of (a) ethanol/1-propanol adsorption selectivity and (b) uptake capacity of ethanol for equimolar ethanol/1-propanol mixtures in TetZB, ZIF-8, and CHA zeolite. The comparisons are based on IAST calculations.

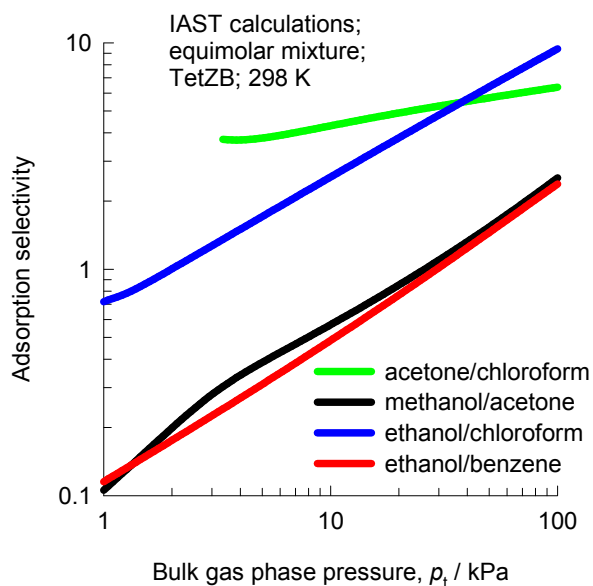


Figure S11. IAST calculations for binary adsorption equilibrium for equimolar acetone/chloroform, methanol/acetone, ethanol/chloroform, and ethanol/benzene at 298 K.

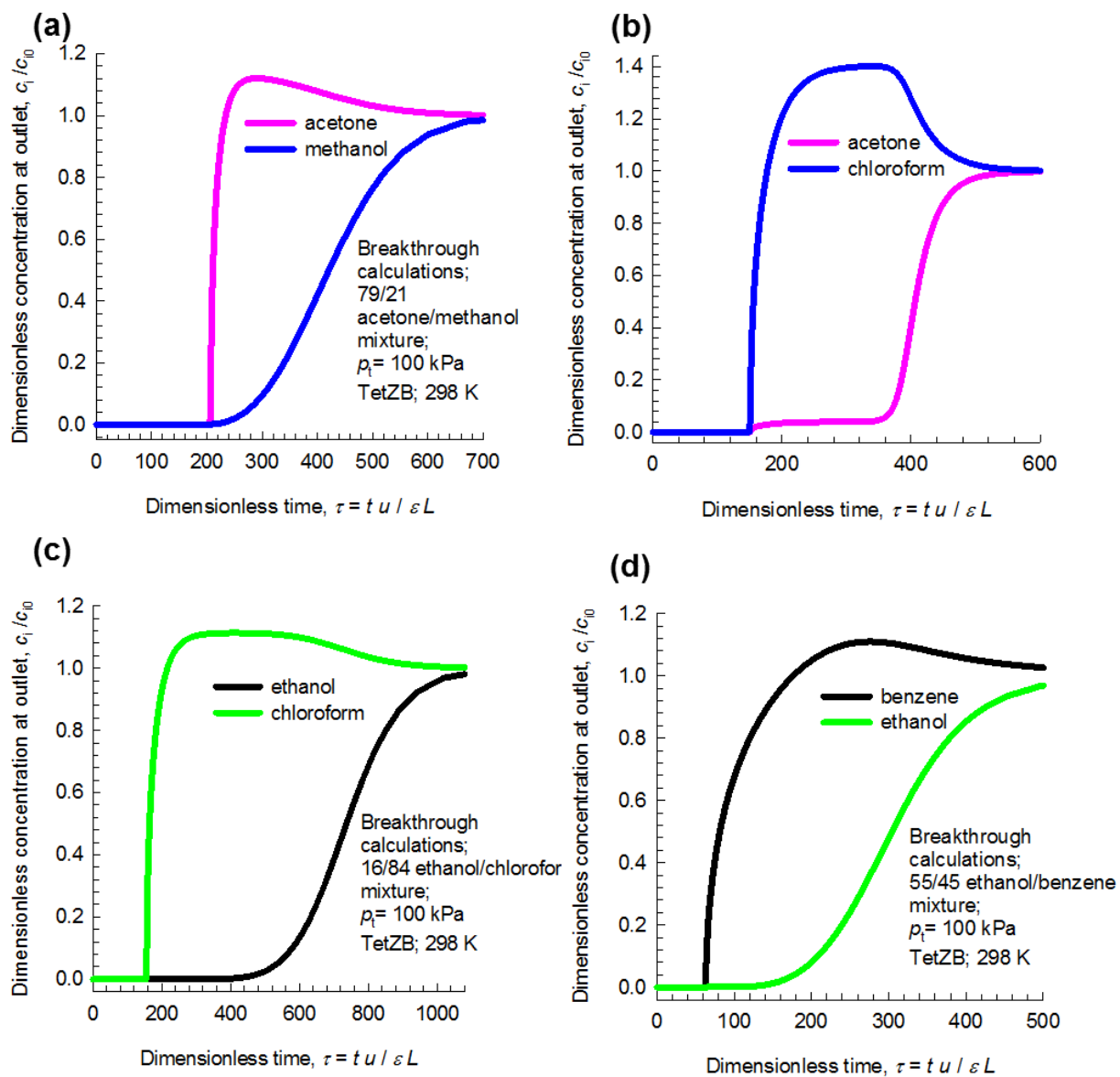


Figure S12. Transient breakthrough simulations for (a) 79/21 acetone/methanol, (b) 34/66 acetone/chloroform, (c) 16/84 ethanol/chloroform, and (d) 55/45 ethanol/benzene mixtures in a fixed-bed adsorber packed with TetZB at 298 K. The total pressure is 100 kPa. Intra-crystalline diffusion effects are accounted for by taking $D_{methanol}/r_c^2 = 2 \times 10^{-3} \text{ s}^{-1}$; $D_{ethanol}/r_c^2 = 1 \times 10^{-3} \text{ s}^{-1}$; $D_{acetone}/r_c^2 = 2 \times 10^{-3} \text{ s}^{-1}$; $D_{chloroform}/r_c^2 = 1 \times 10^{-3} \text{ s}^{-1}$; $D_{benzene}/r_c^2 = 1 \times 10^{-4} \text{ s}^{-1}$.

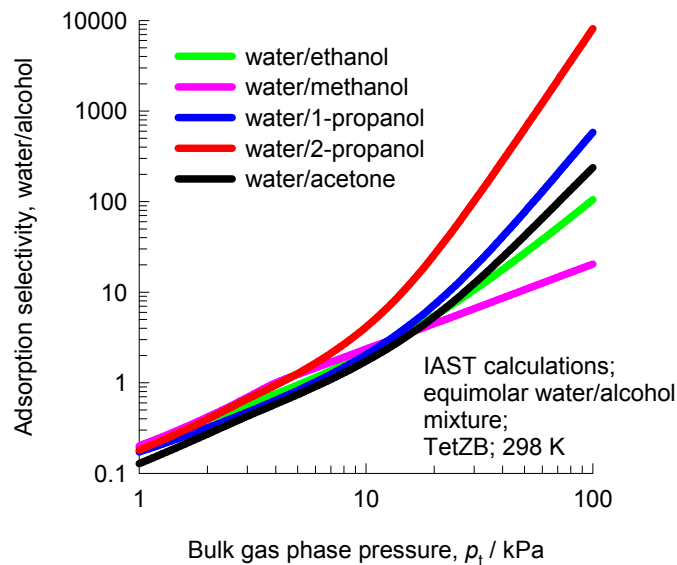


Figure S13: IAST calculations for binary adsorption equilibrium for equimolar water/methanol, water/ethanol, water/1-propanol, water/2-propanol, and water/acetone mixtures in TetZB at 298 K.

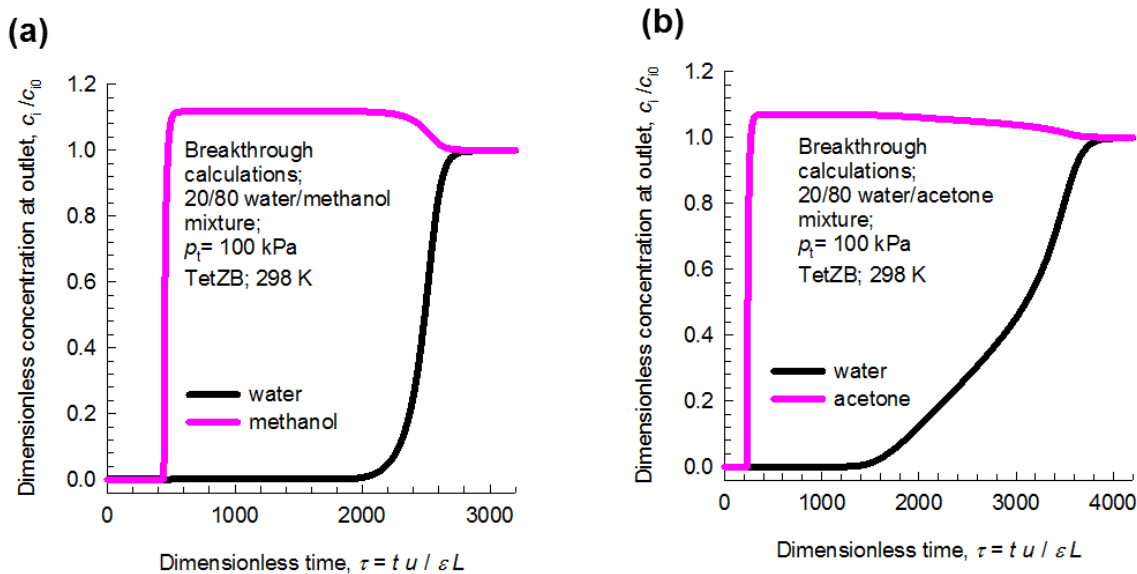


Figure S14: Transient breakthrough simulations for (a) 20/80 water/methanol, and (b) 20/80 water/acetone mixture in a fixed-bed adsorber packed with TetZB at 298 K. The total pressure is

100 kPa. Intra-crystalline diffusion effects are accounted for by taking $D_{water}/r_c^2 = 1 \times 10^{-3} \text{ s}^{-1}$; $D_{methanol}/r_c^2 = 2 \times 10^{-3} \text{ s}^{-1}$; $D_{acetone}/r_c^2 = 2 \times 10^{-3} \text{ s}^{-1}$.

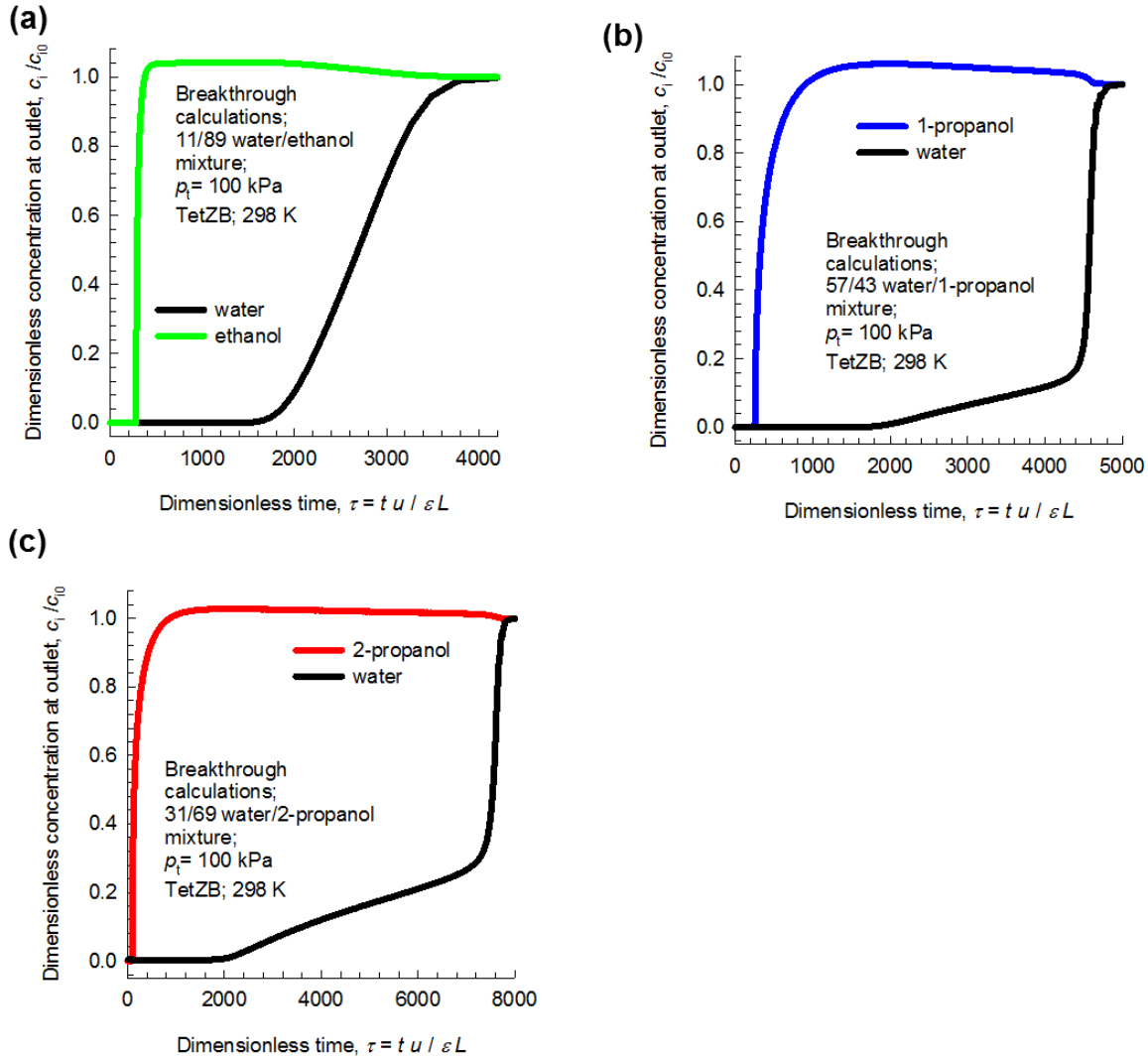


Figure S15: Transient breakthrough simulations for (a) 11/89 water/ethanol, (b) 57/43 water/1-propanol, and (c) 31/69 water/2-propanol mixture in a fixed-bed adsorber packed with TetZB at 298 K. The total pressure is 100 kPa. Intra-crystalline diffusion effects are accounted for by taking $D_{water}/r_c^2 = 1 \times 10^{-2} \text{ s}^{-1}$; $D_{ethanol}/r_c^2 = 1 \times 10^{-3} \text{ s}^{-1}$; $D_{1-propanol}/r_c^2 = 1 \times 10^{-4} \text{ s}^{-1}$; $D_{2-propanol}/r_c^2 = 1 \times 10^{-4} \text{ s}^{-1}$.

Section S6: Schematic of adsorber packed with TetZB

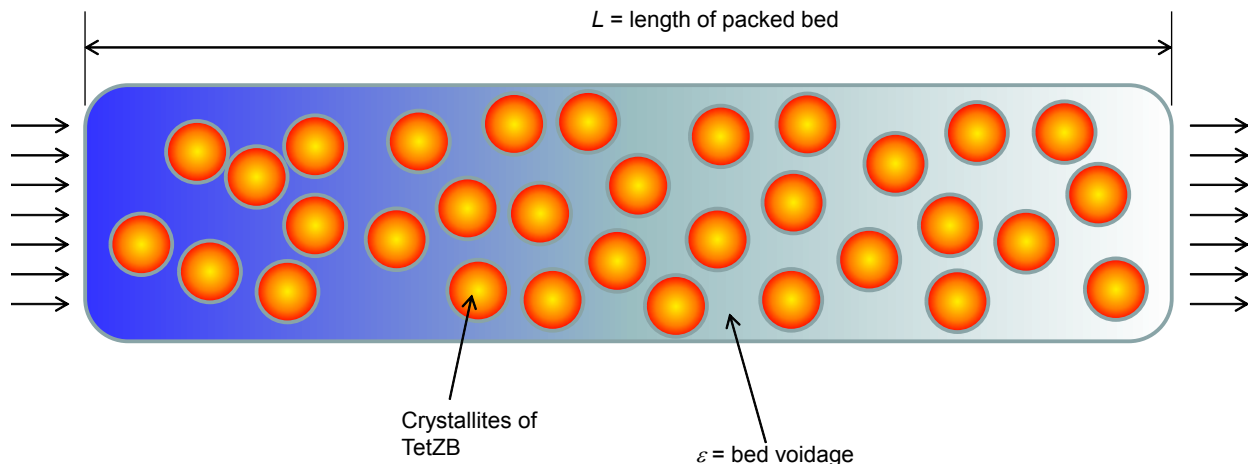


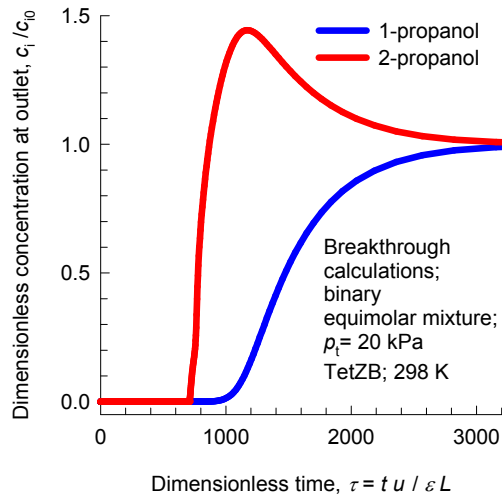
Figure S16: Schematic of adsorber packed with TetZB.

Section S7: Explanation on the Video Animations

In the transient breakthrough simulations, a binary vapor mixture, for example of 1-propanol/1-propanol is injected at time $t = 0$ at the inlet to the fixed bed packed with crystallites of TetZB.

The video animations, also uploaded as ESI, show the transient traversal of the components in the vapor mixture *along the length of the fixed bed* from the inlet (position = 0) to the exit (position = 1). The molar gas-phase concentrations (units mol per m^3) are shown on the y-axis. In all cases, we note that the more weakly adsorbed component is present in higher concentrations in the gas phase, and traverses more quickly from the inlet to the exit. The more strongly adsorbed component is present in lower concentrations in the gas phase, and traverse more slowly.

The more weakly adsorbed component “breaks” through earlier, and we have the familiar breakthrough characteristics, shown below for 1-propanol/2-propanol at total pressure of 20 kPa as shown in Figure 2b of the main paper (shown below).



List of video animations attached:

- Video S1. Video animations of separations of 1-/2-propanol mixture
- Video S2. Video animations of separations of ethanol/1-propanol mixture
- Video S3. Video animations of separations of ethanol/1-propanol mixture
- Video S4. Video animations of separations of ethanol/benzene mixture
- Video S5. Video animations of separations of ethanol/chloroform mixture
- Video S6. Video animations of separations of acetone/methanol mixture
- Video S7. Video animations of separations of acetone/chloroform mixture

Section S8: Notation

b_A	dual-Langmuir-Freundlich constant for species i at adsorption site A, $\text{Pa}^{-\nu_i}$
b_B	dual-Langmuir-Freundlich constant for species i at adsorption site B, $\text{Pa}^{-\nu_i}$
c_i	molar concentration of species i in gas mixture, mol m^{-3}
c_{i0}	molar concentration of species i in gas mixture at inlet to adsorber, mol m^{-3}
\mathcal{D}_i	Maxwell-Stefan diffusivity, $\text{m}^2 \text{s}^{-1}$
L	length of packed bed adsorber, m
n	number of species in the mixture, dimensionless
N_i	molar flux of species i , $\text{mol m}^{-2} \text{s}^{-1}$
p_i	partial pressure of species i in mixture, Pa

p_t	total system pressure, Pa
q_i	component molar loading of species i , mol kg ⁻¹
r_c	radius of crystallite, m
R	gas constant, 8.314 J mol ⁻¹ K ⁻¹
t	time, s
T	absolute temperature, K
u	superficial gas velocity in packed bed, m s ⁻¹
v	interstitial gas velocity in packed bed, m s ⁻¹

Greek letters

ε	voidage of packed bed, dimensionless
Θ_i	loading of species i , molecules per unit cell
ρ	framework density, kg m ⁻³
τ	time, dimensionless

Subscripts

i	referring to component i
t	referring to total mixture

Section S9: References

1. P. K. Thallapally, J. Tian, M. R. Kishan, C. A. Fernandez, S. J. Dalgarno, P. B. McGrail, J. E. Warren and J. L. Atwood, *J Am Chem Soc*, 2008, **130**, 16842-+.
2. M. Sadakiyo, T. Yamada and H. Kitagawa, *J Am Chem Soc*, 2011, **133**, 11050-11053.
3. (a) R. Krishna and J. M. van Baten, *Langmuir*, 2010, **26**, 3981-3992; (b) R. Krishna and J. M. van Baten, *Langmuir*, 2010, **26**, 8450-8463; (c) R. Krishna and J. M. van Baten, *Langmuir*, 2010, **26**, 10854-10867; (d) R. Krishna and J. M. van Baten, *J. Membr. Sci.*, 2010, **360**, 476-482.
4. (a) E. D. Bloch, W. L. Queen, R. Krishna, J. M. Zadrozny, C. M. Brown and J. R. Long, *Science*, 2012, **335**, 1606-1610; (b) Z. R. Herm, B. M. Wiers, J. M. Van Baten, M. R. Hudson, P. Zajdel, C. M. Brown, N. Maschiochi, R. Krishna and J. R. Long, *Science*, 2013, **340**, 960-964; (c) C. Gücüyener, J. van den Bergh, J. Gascon and F. Kapteijn, *J. Am. Chem. Soc.*, 2010, **132**, 17704-17706; (d) J. Yang, R. Krishna, J. Li and J. Li, *Microporous Mesoporous Mater.*, 2014, **184**, 21-27; (e) R. Krishna, *Micropor Mesopor Mat*, 2014, **185**, 30-50.
5. R. Krishna and J. R. Long, *J. Phys. Chem. C*, 2011, **115**, 12941-12950.
6. R. Krishna and R. Baur, *Sep. Purif. Technol.*, 2003, **33**, 213-254.
7. A. L. Myers and J. M. Prausnitz, *A.I.Ch.E.J.*, 1965, **11**, 121-130.